scientific reports

Check for updates

OPEN

Deficiencies in methionine, tryptophan, and niacin remodels intestinal transcriptome and gut microbiota in female mice

Tomoaki Hara[1], Sikun Meng[1], Daisuke Motooka[2], Yasuko Arao[1], Yoshiko Saito[1], Sarah Rennie[3], Shizuka Uchida[4], Ken Ofusa[1,5], Takahiro Arai[1,6], Masamitsu Konno[1,7], Taroh Satoh[8] & Hideshi Ishii[1]✉

Caloric restriction is well-established as a robust intervention that may extend lifespan and improve metabolic health across species with effects that are increasingly attributed to both host metabolic remodeling and alterations in the gut microbiota. Recent studies suggest that restricting specific dietary components can replicate these benefits. While methionine and branched-chain amino acid restriction improve metabolism and modulate the gut microbiome, the effects of other nutrients remain unclear. Here, we explore the effects of methionine, tryptophan and niacin deprivation on host intestinal gene expression and gut microbiota using female murine models. Through transcriptomic analysis of the intestinal tissue, we found that transient dietary restriction of methionine, tryptophan, and niacin induced significant changes in intestinal gene expression, particularly in genes involved in oxidative phosphorylation and ATP production. Single-cell analysis revealed that dietary restriction of those nutrients led to an increase in intestinal immune cell populations. Gut microbiota profiling also revealed that transient deprivation of those nutrients resulted in changes in microbial composition, with an increased relative abundance of *Lactobacillus* species observed in some cases. Our findings highlight the potential of targeted nutrient restriction as a strategy to reprogram host-microbiome interactions.

Keywords Methionine restriction (MR), Tryptophan and niacin restriction (TNR), Methionine, Tryptophan, And niacin restriction (MTNR), Intestinal transcriptome, Gut microbiota

Calorie restriction (CR), defined as a sustained reduction in caloric intake without malnutrition, has long been recognized for its ability to extend lifespan and improve healthspan across species[1]. In rodents, CR delays the onset of age-related diseases and promotes longevity[2–5]. Human studies, including the CALERIE trial, have shown that two years of moderate CR leads to sustained weight loss, reduced metabolic rate, and decreased oxidative stress[6–9]. These changes support the rate-of-living and oxidative damage theories of aging and are associated with improved cardiometabolic markers, such as insulin sensitivity, blood pressure, and inflammation[10,11]. Meta-analyses have further supported the clinical benefits of CR[12]. Among nutrient-specific strategies, restriction of methionine and branched-chain amino acids (BCAAs) has gained attention. Methionine restriction (MR) extends lifespan and reduces mitochondrial oxidative stress via activation of protective pathways[13–16]. BCAA restriction, particularly in male mice, improves metabolic health and longevity, likely through inhibition of mTORC1 and downregulation of p21[17,18]. These interventions also modulate the gut microbiota, influencing

[1]Department of Medical Data Science, Center of Medical Innovation and Translational Research, Osaka University Graduate School of Medicine, Yamadaoka 2-2, Suita, Osaka 565-0871, Japan. [2]Genome Information Research Center, Research Institute for Microbial Diseases, Osaka University, Suita, Osaka 565-0871, Japan. [3]Section for Computational and RNA Biology, Department of Biology, University of Copenhagen, Copenhagen, Denmark. [4]Center for RNA Medicine, Department of Clinical Medicine, Aalborg University, DK-2450, Copenhagen SV, Denmark. [5]Prophoenix Division, Food and Life-Science Laboratory, IDEA Consultants, Inc., Osaka 559-0034, Japan. [6]Unitech Co., Ltd., Kashiwa, Chiba 277-0005, Japan. [7]Biological Data Science Research Group, Cellular and Molecular Biotechnology Research Institute, National Institute of Advanced Industrial Science and Technology, 2-3-26 Aomi, Koto, Tokyo 135-0064, Japan. [8]Department of Gastroenterological Surgery, Osaka University Graduate School of Medicine, Yamadaoka 2-2, Suita 565-0871, Japan. ✉email: hishii@gesurg.med.osaka-u.ac.jp

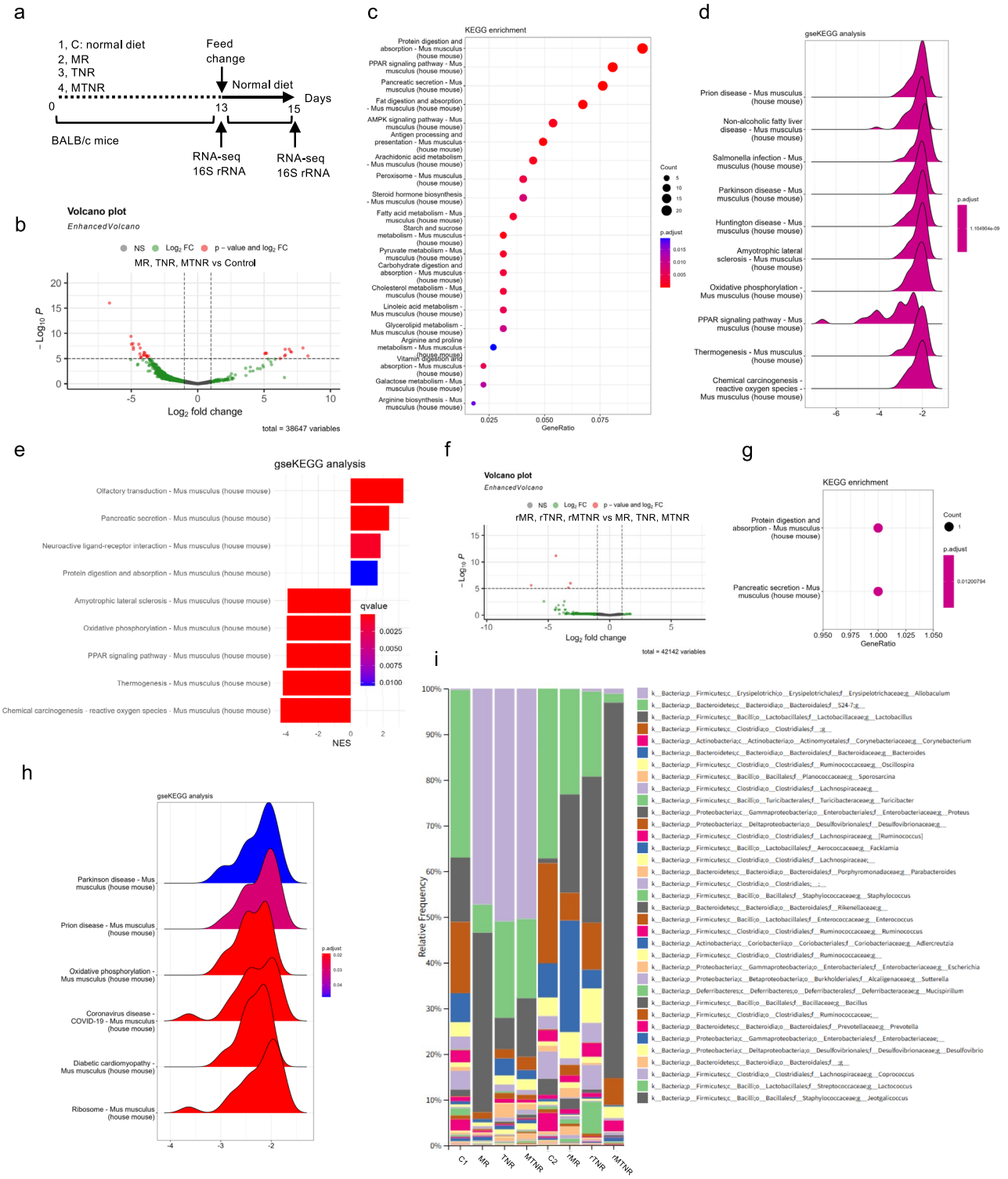

host metabolism, intestinal permeability, and inflammation[19–22]. Despite promising findings, the effects of restricting other essential nutrients remain underexplored and require further investigation to better understand their potential in promoting healthy aging.

Tryptophan, an essential amino acid, is vital for serotonin synthesis, immune regulation, and kynurenine metabolism[23]. As humans cannot produce it, dietary intake is crucial. Tryptophan deficiency, caused by poor diet, disease, or metabolic disturbances, contributes to pellagra, depression, fatigue, and gut dysbiosis-related inflammation[24–26]. Niacin (vitamin B3), which can also be synthesized from tryptophan in the body, is essential for the synthesis of NAD^+ and $NADP^+$, supporting energy metabolism and DNA repair[27,28]. While pellagra, marked by dermatitis, diarrhea, and dementia, is rare in developed countries, subclinical deficiency remains prevalent among alcoholics, cancer patients, and those in post-conflict areas[29–31]. Niacin deficiency has been shown to induce inflammation in the intestine, whereas niacin supplementation has been found to alleviate such inflammation[32]. While it is well established that chronic deficiency of tryptophan or niacin has detrimental

◀**Fig. 1**. Deficiency of methionine, tryptophan, and niacin remodels intestinal transcriptome and gut microbiota in BALB/c mice. (**a**) Schematic diagram of the experiment. BALB/c mice were fed methionine-restricted (MR), tryptophan- and niacin-restricted (TNR), or methionine-, tryptophan-, and niacin-restricted (MTNR) diets. Intestinal RNA-seq and fecal 16S rRNA sequencing were performed after the deficiency diets and after returning to the standard diet. Mice in the C, MR, and TNR groups were housed with n = 5 per group, the MTNR group with n = 6, the rMR and rTNR groups with n = 4 each, and the rMTNR group with n = 1. RNA-seq was performed using one mouse per group. Fecal samples were collected from each cage. The rMR, rTNR, and rMTNR groups refer to mice that were fed the respective deficient diets followed by two days of standard chow. **b**-**e**. The gene expression characteristics of the MR, TNR, and MTNR groups compared to the control diet. (**b**) Volcano plots display the distribution of gene expression changes in the MR, TNR, and MTNR groups relative to the control group. The x-axis represents $\log_2$ fold change, and the y-axis shows the adjusted p-value (padj). Analysis was conducted using DESeq2 and visualized using the EnhancedVolcano package. (**c**) KEGG pathway enrichment analysis was performed using the enrichKEGG function in the clusterProfiler package. Differentially expressed genes were converted to Entrez Gene IDs and analyzed against the mouse KEGG pathway database (mmu). The top 20 significantly enriched pathways (p-value < 0.05) are shown as a dot plot. Dot size represents the number of genes involved in each pathway, and color indicates the adjusted p-value. (**d**) KEGG pathway enrichment analysis using the gseKEGG function. The top 10 enriched KEGG pathways are shown as a ridge plot. (**e**) Top four upregulated and top five downregulated KEGG pathways based on normalized enrichment scores (NES). Pathways are ranked by absolute NES, and the bar plot shows the direction and magnitude of enrichment, with color indicating q-value significance. **f**-**g**. The gene expression characteristics of the rMR, rTNR, and rMTNR groups compared to the MR, TNR, and MTNR groups. (**f**) Volcano plots display the distribution of gene expression changes in the rMR, rTNR, and rMTNR groups relative to the MR, TNR, and MTNR groups. The x-axis represents $\log_2$ fold change, and the y-axis shows the adjusted p-value (padj). Analysis was conducted using DESeq2 and visualized using the EnhancedVolcano package. (**g**) KEGG pathway enrichment analysis was performed using the enrichKEGG function in the clusterProfiler package. Differentially expressed genes were converted to Entrez Gene IDs and analyzed against the mouse KEGG pathway database (mmu). The detected two significantly enriched pathways (p-value < 0.05) are shown as a dot plot. Dot size represents the number of genes involved in each pathway, and color indicates the adjusted p-value. (**h**) KEGG pathway enrichment analysis using the gseKEGG function. The detected six enriched KEGG pathways are shown as a ridge plot. (**i**) Gut microbiota composition of control, nutrient-deficient diet groups (MR, TNR and MTNR) and recovery groups (rMR, rTNR and rMTNR) analyzed at taxonomic level 6 using QIIME2.

effects on health, it remains largely unexplored whether recovery from transient deficiency could elicit beneficial effects similar to those observed with CR. Given that tryptophan is a precursor for both serotonin and niacin, and that niacin itself plays a key role in redox metabolism and mitochondrial function[33,34], their combined restriction may profoundly alter metabolic pathways.

In our previous work using a mouse model of inflammatory bowel disease (IBD), we demonstrated that dietary restriction of methionine, tryptophan, and niacin led to marked shifts in gut microbiota composition and immune gene expression, accompanied by enhanced lipid catabolism and proteolysis[35]. These findings highlighted that deprivation of the nutrients can exert systemic effects beyond nutrient balance, contributing to host–microbe interactions and inflammation regulation. Building on these insights, the present study explores how the restriction of tryptophan and niacin—both essential for energy metabolism and nicotinamide adenine dinucleotide (NAD^+) synthesis[36]—affects host intestinal gene expression and gut microbiota in the absence of overt inflammatory stimuli. We prepared three types of nutrient-deficient diets: a methionine-deficient diet, a tryptophan and niacin-deficient diet, and a combined methionine, tryptophan, and niacin-deficient diet. Female mice were fed each diet for a defined period, followed by a return to a normal diet. We then analyzed intestinal gene expression and the gut microbiota. In this study, we demonstrate that dietary deprivation of methionine, tryptophan, and niacin induces profound changes in both host intestinal transcriptome and gut microbiota composition. These observations underscore the intertwined roles of methionine-, tryptophan-, and niacin-deficient diets in shaping host intestinal transcriptomic remodeling and gut microbial dynamics.

Results

Tryptophan and niacin restriction remodels intestinal gene expression and microbiota composition in BALB/c mice

NAD^+, an essential cofactor for energy metabolism, is synthesized from tryptophan and niacin. Therefore, we hypothesized that dietary restriction of tryptophan and niacin (TNR) would profoundly alter intestinal gene expression and microbiota composition. To test this, we fed BALB/c mice with normal diet, methionine-restricted diet (MR), tryptophan and niacin-restricted diet (TNR), or a combination-restricted diet lacking methionine, tryptophan, and niacin (MTNR) for 13 days. We confirmed that the nutrient-deficient diets were consumed by the mice (Supplementary data S1). We then analyzed intestinal gene expression by RNA-seq and assessed the gut microbiota via 16S rRNA profiling (Fig. 1a). Since it has been reported that a methionine- and choline-deficient (MCD) diet alters the expression of pro-inflammatory chemokines after two weeks of feeding[37], we considered that a two-week nutrient-deficient diet would be sufficient to induce changes in intestinal gene expression. To identify gene expression changes common to MR, TNR, and MTNR, we first compared their gene expression profiles with those of the control group. Gene expression analysis revealed widespread transcriptional changes in the restricted diet groups compared to the control group, with particularly pronounced alterations in genes

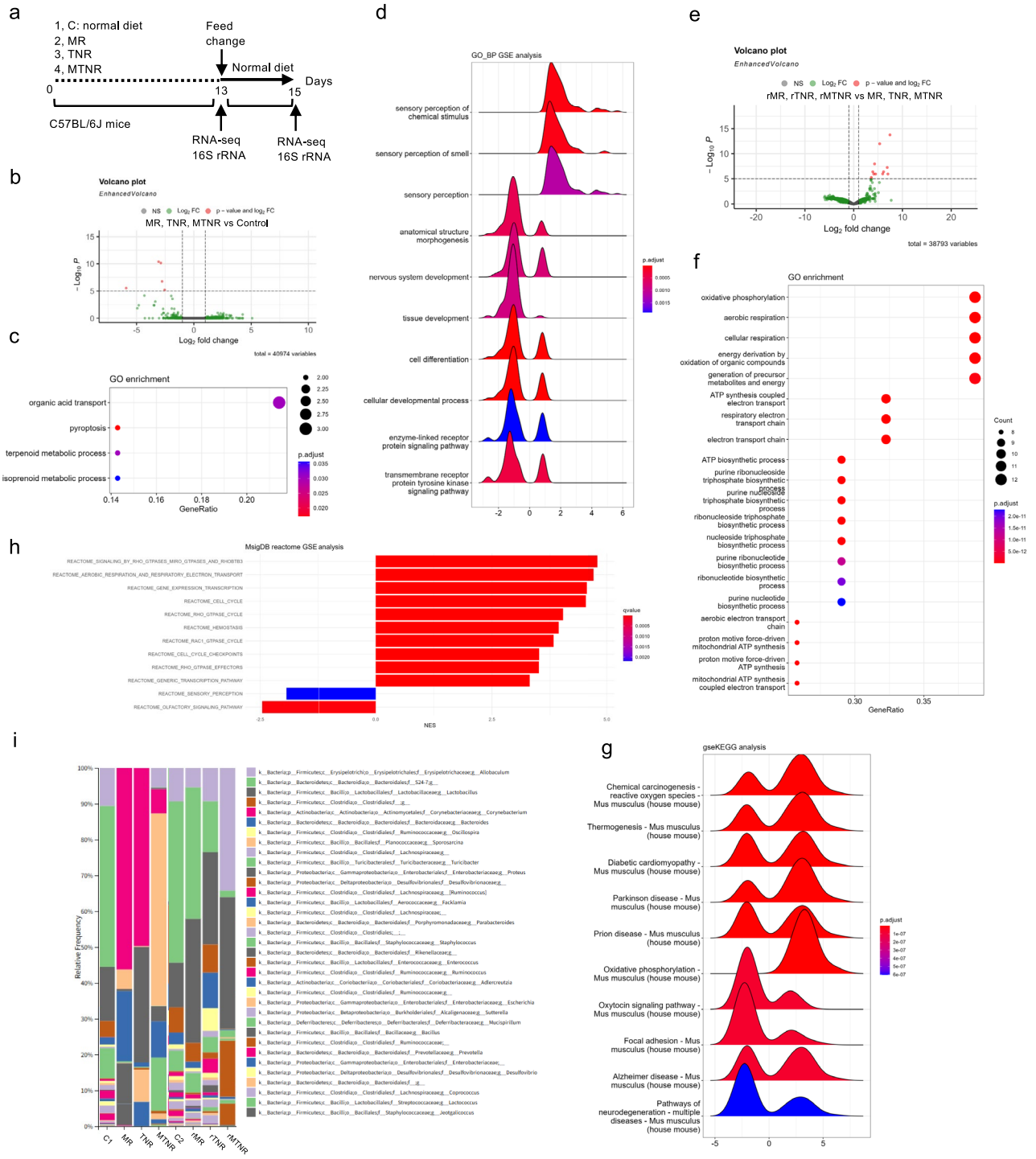

related to protein and fat digestion (Fig. 1b, c, and Extended Data Fig. 1a). Gene set enrichment analysis (GSEA) of KEGG pathways indicated downregulation of the PPAR signaling pathway and oxidative phosphorylation under nutrient-deficient conditions (Fig. 1d, e). To evaluate the effects of transient nutrient restriction, mice were returned to a normal diet for 2 days following the 13-day restriction (rMR, rTNR, rMTNR). To identify gene expression changes common to rMR, rTNR, and rMTNR, we compared their gene expression profiles with those of MR, TNR, and MTNR. RNA-seq analyses revealed that this temporary restriction led to distinct gene expression profiles, notably in pathways related to protein digestion and pancreatic secretion (Fig. 1f and g). GSEA showed persistent suppression of oxidative phosphorylation and disease pathways including diabetic cardiomyopathy, COVID-19, prion disease, and Parkinson's disease (Fig. 1h). These results demonstrate that short-term dietary restriction of tryptophan and niacin induces marked transcriptional remodeling in the intestine.

To examine the impact of each dietary restriction on intestinal gene expression, we performed t-SNE analysis of the transcriptomic profiles, revealing that mice fed a normal diet, restricted diets (MR, TNR, MTNR), and

◀**Fig. 2**. Deficiency of methionine, tryptophan, and niacin leads to strain-specific gut transcriptomic and microbial changes in C57BL/6 J mice. (**a**) Schematic diagram of the experiment. The same experiment as in Fig. 1 was conducted using C57BL/6 J mice. Mice were housed as follows: C and MR groups with $n = 4$, TNR with $n = 5$, MTNR with $n = 8$, rMR with $n = 3$, rTNR with $n = 4$, and rMTNR with $n = 2$. RNA-seq was performed using one mouse per group. Fecal samples were collected from each cage. **b**-**d**. The gene expression characteristics of the MR, TNR, and MTNR groups compared to the control diet. (**b**) Volcano plots display the distribution of gene expression changes in the MR, TNR, and MTNR groups relative to the control group. The x-axis represents $\log_2$ fold change, and the y-axis shows the adjusted p-value (padj). Analysis was conducted using DESeq2 and visualized using the EnhancedVolcano package. (**c**) Gene Ontology (GO) biological processes (BP) among the differentially expressed genes using the enrichGO function from the clusterProfiler package. Mouse gene Entrez IDs were used as input, and enrichment was assessed against the org.Mm.eg.db database. Significantly enriched GO terms were selected using Benjamini–Hochberg adjusted p-values and q-values less than 0.05. (**d**) Gene Set Enrichment Analysis (GSEA) of Gene Ontology Biological Processes (GO-BP) was performed using the gseGO function from the clusterProfiler package. Ranked gene lists based on differential expression were analyzed against the mouse GO-BP database (org.Mm.eg.db), identifying significantly enriched biological pathways ($p < 0.05$) with gene set sizes between 20 and 500. **e**-**h**. The gene expression characteristics of the rMR, rTNR, and rMTNR groups compared to the MR, TNR, and MTNR groups. (**e**) Volcano plots display the distribution of gene expression changes in the rMR, rTNR, and rMTNR groups relative to the MR, TNR, and MTNR groups. The x-axis represents $\log_2$ fold change, and the y-axis shows the adjusted p-value (padj). Analysis was conducted using DESeq2 and visualized using the EnhancedVolcano package. (**f**) Gene Ontology (GO) biological processes (BP) among the differentially expressed genes using the enrichGO function from the clusterProfiler package. Mouse gene Entrez IDs were used as input, and enrichment was assessed against the org.Mm.eg.db database. Significantly enriched GO terms were selected using Benjamini–Hochberg adjusted p-values and q-values less than 0.05. (**g**) KEGG pathway enrichment analysis using the gseKEGG function. The top 10 enriched KEGG pathways are shown as a ridge plot. (**h**) Gene Set Enrichment Analysis (GSEA) was performed using the Reactome pathway gene sets from the Mouse MSigDB collection (m2.cp.reactome.v2024.1.Mm.entrez.gmt). Enrichment was conducted with the GSEA function using ranked gene lists derived from differential expression analysis. The top 10 positively and negatively enriched pathways based on normalized enrichment score (NES) were visualized. Color gradients represent q-values, indicating the statistical significance of pathway enrichment. (**i**) Gut microbiota composition of control, nutrient-deficient diet groups (MR, TNR and MTNR) and recovery groups (rMR, rTNR and rMTNR) analyzed at taxonomic level 6 using QIIME2.

recovery diets following restriction (rMR, rTNR, rMTNR) each exhibited distinct and characteristic gene expression patterns (Extended Data Fig. S1b). In the MR and TNR groups, we observed robust regulation of genes involved in autophagy and proteolysis, along with downregulation of oxidative phosphorylation and neurological disease pathways (Extended Data Fig. 1c–h). In contrast, the TNR group uniquely showed significant alterations in lipid metabolism-related genes and upregulation of proteolytic and methionine metabolic signaling, without suppression of oxidative phosphorylation as seen in the MR group (Extended Data Fig. 1i–k). Notably, In the recovery groups (rMR and rTNR), alterations in the expression of autophagy-related genes and a decrease in oxidative phosphorylation, which were observed in the MR and TNR groups, were detected (Extended Data Fig. 2a–f). In rMTNR, gene changes were associated with purine metabolism, repression of PPAR signaling, and decreased oxidative phosphorylation (Extended Data Fig. 2g–i). These results suggest that transient dietary restriction might leave a lasting transcriptional imprint on intestinal tissue.

Previous studies have shown that transient dietary restriction followed by refeeding promotes the expansion of intestinal *Lactobacillus* in mice[38]. To investigate whether tryptophan and niacin deficiency induces comparable microbial dynamics, we performed 16S rRNA gene profiling on fecal samples collected from mice subjected to each dietary regimen. Nutrient restriction induced significant shifts in microbial composition, with an increased relative abundance of *Lactobacillus* observed in the rMTNR group (Fig. 1i). To identify bacterial taxa associated with each dietary intervention, we performed multivariate analysis using Multivariate Association with Linear Models 2 (MaAsLin2). This analysis revealed that the *Christensenellaceae* family was enriched in the rMR group, while *Candidatus Arthromitus* was associated with both the TNR and rTNR groups. In the MTNR group, significant associations were observed with multiple taxa, including *Actinomyces*, *Chryseobacterium*, *Paenibacillus*, members of the *Neisseriaceae* family, and *Enterobacteriaceae* (Extended Data Fig. 3). In the rMTNR group, Chao1, Simpson, Shannon indices, and the number of Amplicon Sequence Variants (ASVs) were lower compared to the other samples (Supplementary data S2). These results suggest that nutrient restriction–induced alterations in the gut microbiota might be highly dependent on the specific deprivation of methionine, tryptophan, and niacin.

Dietary restriction induces strain-specific transcriptional and microbial shifts in C57BL/6 mice

It has been reported that BALB/c mice have a gut microbiota dominated by Bacteroidetes, whereas C57BL/6 mice have a microbiota dominated by Firmicutes[39]. To determine whether similar effects occur in other mouse strains, we replicated the dietary intervention in C57BL/6 (BL6) mice (Fig. 2a). To identify gene expression changes common to MR, TNR, and MTNR, we compared their gene expression profiles with those of the control group. Although the magnitude of transcriptional change was less than in BALB/c mice, differentially expressed genes were still detected between control and restriction groups (MR, TNR, MTNR), particularly in pathways related to organic acid transport, pyroptosis, and terpenoid and isoprenoid metabolism. Nutrient-restricted

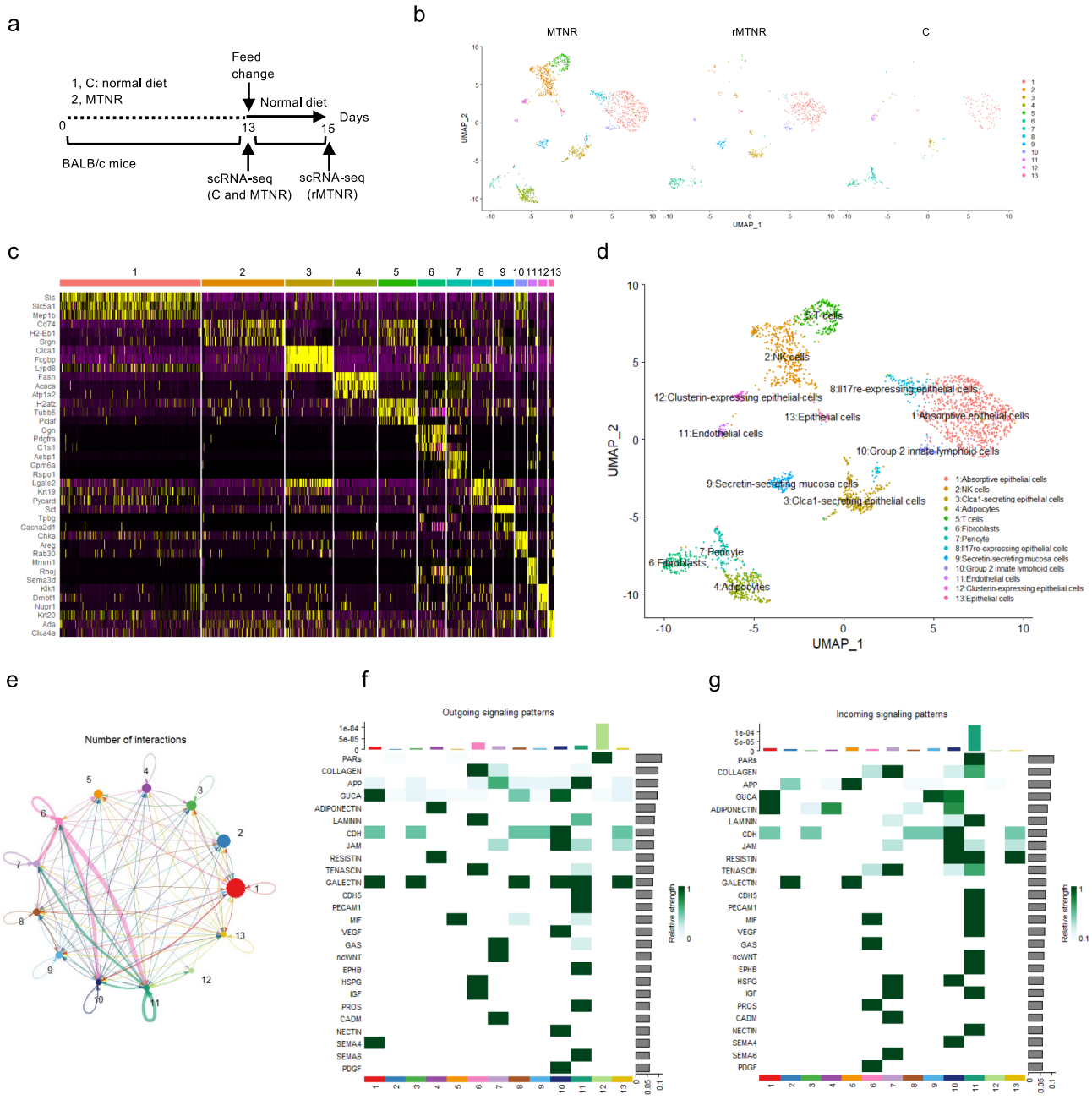

Fig. 3. Single-cell RNA-sequencing (scRNA-seq) reveals cell type–specific responses to dietary methionine, tryptophan, and niacin restriction in the intestine. (**a**) Schematic diagram of the experiment. Following the same schedule as in Fig. 1, BALB/c mice were recovered from the MTNR diet by switching to a normal diet (rMTNR). scRNA-seq was performed on intestinal cells from the normal diet (C), MTNR, and rMTNR groups. The mice used for scRNA-seq were the same as those used in the experiment shown in Fig. 1, with one mouse analyzed per condition. (**b**) Distribution of cells in UMAP for each condition. Gene expressions of control, MTNR and rMTNR were compressed by UMAP after integration of data obtained in the three conditions. (**c**) Heatmap illustrating the expression levels of the top three marker genes in each cluster across different conditions. Marker genes were identified using the FindAllMarkers function in Seurat. (**d**) Cell types of each cluster. **e**–**f**. Cell–cell communication analysis with CellChat package. (**e**) Circle plot illustrating the number of inferred intercellular communications between clusters, generated using netVisual_circle. (**f**) Heatmap showing outgoing signaling roles of each cluster, produced by netAnalysis_signalingRole_heatmap with the "outgoing" parameter. (**g**) Heatmap showing incoming signaling roles of each cluster, produced by netAnalysis_signalingRole_heatmap with the "incoming" parameter.

groups exhibited increased responses to chemical stimuli and decreased cellular biosynthetic process (Fig. 2b–d). To identify gene expression changes common to rMR, rTNR, and rMTNR, we compared their gene expression profiles with those of MR, TNR, and MTNR. Recovery groups (rMR, rTNR, rMTNR) displayed prominent changes in oxidative phosphorylation and ATP synthesis-related genes, alongside upregulation of oxidative phosphorylation and cell cycle pathways (Fig. 2e–h). Heatmaps and t-SNE plots of gene expression revealed similarities in transcriptional patterns between MR and TNR, and between rTNR and rMTNR (Extended Data Fig. 4a, 4b). Compared to the control diet, MR led to pronounced alterations in genes associated with nucleic acid metabolism, accompanied by downregulation of oxidative phosphorylation and the COVID-19 signaling pathway. However, in contrast to findings in BALB/c mice, pathways related to neurological disorders were not significantly suppressed (Extended Data Fig. 4c–e). In TNR group, similar transcriptomic changes were observed, including robust regulation of nucleic acid metabolism genes and suppression of both oxidative phosphorylation and the COVID-19 pathway. Notably, consistent with observations in BALB/c mice, TNR also resulted in the downregulation of neurological disease pathways (Extended Data Fig. 4f.–h). MTNR triggered shifts in nucleotide metabolism genes and enhanced oxidative phosphorylation and fatty acid metabolism (Extended Data Fig. 4i–k). These results imply that dietary restriction of tryptophan and niacin might confer greater neuroprotective benefits than methionine restriction alone. In the recovery groups, rMR showed enhanced expression of genes involved in nucleotide and lipid metabolism (Extended Data Fig. 5a–c). rTNR also exhibited upregulation of oxidative phosphorylation and fatty acid metabolism, with suppression of MAPK and PI3K/AKT/mTOR pathways (Extended Data Fig. 5d–f). rMTNR was characterized by altered expression of metal ion and organic transporter genes, upregulation of the TCA cycle and ROS pathways, and suppression of the nicotine addiction pathway (Extended Data Fig. 5g–i). Gut microbiota profiling via 16S rRNA analysis revealed similar patterns to those observed in BALB/c mice, including enrichment of *Lactobacillus* in the rMTNR group (Fig. 2i). MaAsLin2 analysis identified strain-specific microbial signatures, including *Natronobacillus* in MR, *Bilophila* in rTNR, and *Pseudomonas* in MTNR (Extended Data Fig. 6). These findings collectively demonstrate that MR, TNR, and MTNR diets significantly reshape host transcriptional landscapes and gut microbial communities, producing distinct host–microbiota states under each condition.

Intestinal single-cell profiling reveals fibroblast- and immune-driven signal rewiring under MTNR or recovery conditions

To investigate gene expression changes at the cellular level, we performed single-cell RNA sequencing (scRNA-seq) on intestinal tissues from mice fed a control diet, the MTNR diet, or following recovery from MTNR (rMTNR) (Fig. 3a). The cellular composition varied across conditions, and distinct marker genes were identified for each cluster (Fig. 3b and c). Based on marker gene expression, we annotated the clusters as various intestinal cell types, including epithelial cells, immune cells, and fibroblasts (Fig. 3d). Notably, Group 2 innate lymphoid cells (ILC2s), which are key regulators of mucosal immunity and tissue remodeling through the production of type 2 cytokines such as IL-5 and IL-13[40], were specifically enriched under MTNR and rMTNR conditions. This observation raises the possibility that ILC2s might contribute to host adaptation to nutrient-deficient states. To explore intercellular communication, we conducted CellChat analysis, which revealed extensive signaling networks across cell types. Notably, fibroblasts (cluster 6), pericytes (cluster 7), ILC2s (cluster 10), and endothelial cells (cluster 11) emerged as central hubs for signal transmission (Fig. 3e). Further analysis of outgoing and incoming signaling patterns indicated that these cell populations were highly active in both sending and receiving signals, particularly those related to extracellular matrix organization and cell adhesion (Fig. 3f and g). These findings suggest that transient restriction of methionine, tryptophan, and niacin might not only reshape the cellular landscape of the intestine but also engage specific immune populations, notably ILC2s, as part of the adaptive response to nutrient stress.

Fecal microbiota transplantation (FMT) from recovery diets modulates host immunity and metabolism in MTNR-treated mice

Recent studies have suggested that fecal microbiota transplantation (FMT) may enhance host health through modulation of gut microbiota[41]. To investigate whether the gut microbiota reconstructed during dietary recovery harbors such beneficial potential, we transplanted fecal samples from recovery-phase mice (rMR, rTNR, and rMTNR) into MTNR-fed recipient mice and assessed the resulting host intestinal gene expression and gut microbiota (Fig. 4a). Based on the experiments shown in Fig. 1 and Fig. 2, which revealed changes in the gut microbiota after two days of standard diet following the deficiency diets, fecal samples used for FMT were collected under those conditions.

In addition, since previous reports have shown that changes in host gene expression and gut microbiota can occur two days after FMT[42], we performed RNA-seq and 16S rRNA profiling two days after the initial transplantation. Compared to the control diet group, mice that received fecal microbiota transplantation (FMT) exhibited marked transcriptional changes in immune-related genes, characterized by suppression of immune system pathways and upregulation of nucleotide metabolism (Fig. 4b–e). Analysis of the gut microbiota in FMT recipient mice revealed distinct microbial profiles in groups transplanted with microbiota from recovery-phase donors, compared to those receiving control feces (Fig. 4f). These results suggest that feces from the recovery groups of tryptophan and niacin deficiency might possess the ability to modulate the gut microbiota.

Previous studies have reported that changes in metabolic profiles following FMT can influence therapeutic outcomes[43]. Therefore, we conducted metabolomic profiling of feces from the FMT recipient groups to investigate how fecal transplantation influenced the metabolite composition of the intestinal tract. Metabolomic profiling of the FMT recipient groups showed unique metabolic signatures in each condition—control, rMR, rTNR, and rMTNR FMT—while the rTNR and rMTNR FMT groups shared overlapping metabolic features (Fig. 5a and Extended Data Fig. 7a). Amino acid profiling revealed condition-specific alterations across FMT groups:

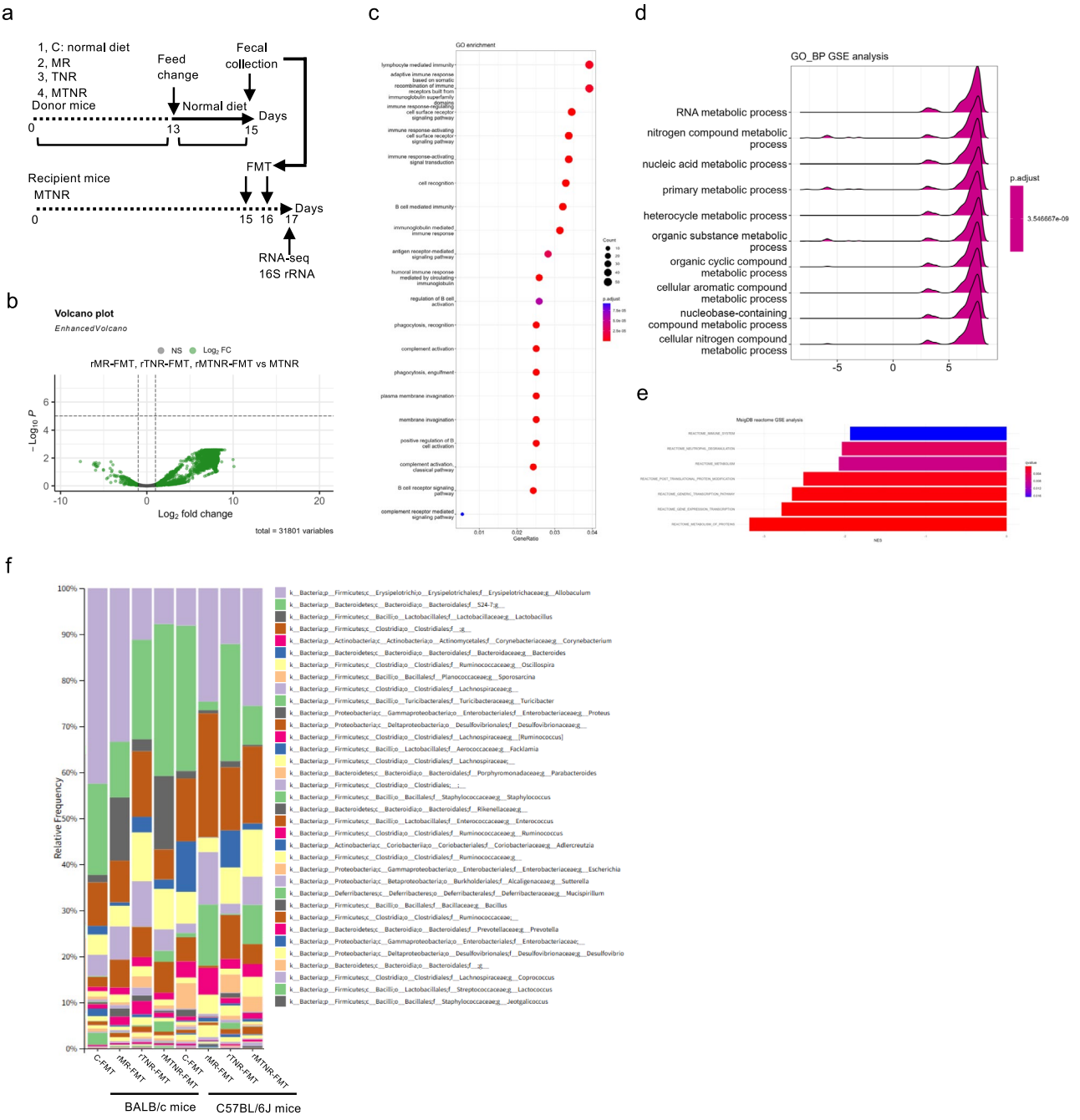

arginine levels were markedly reduced in the rMR FMT group, asparagine was significantly decreased in the rTNR FMT group, and conversely, asparagine levels were markedly elevated in the rMTNR FMT group (Fig. 5b). Pathway-wide metabolomic analysis indicated that most of the detected metabolites were intermediates of the tricarboxylic acid (TCA) cycle or associated with nucleotide metabolism (Fig. 5c). Although fluctuations in the levels of individual TCA cycle intermediates were observed across groups, key metabolites such as pyruvic acid and malic acid remained abundant in all conditions, suggesting that TCA cycle function might remain intact following fecal transplantation (Extended Data Fig. 7b). In contrast, levels of guanine were decreased in the rMR and rTNR FMT groups, and this reduction was further pronounced in the rMTNR FMT group (Extended Data Fig. 8). Similarly, adenine levels progressively declined across rMR-, rTNR-, and rMTNR-FMT groups, with the greatest reduction observed in the rMTNR-FMT mice (Extended Data Fig. 9), indicating cumulative suppression of purine metabolism by recovery-phase microbial communities.

Gut microbiota remodeling by nutrient-deficient diets occurs irrespective of restriction duration and is transferable by fecal transplantation

To examine whether the alterations in gut microbiota are influenced by the duration of nutrient restriction and the restoration of a normal diet, we modified the period of dietary deprivation to 14, 9, or 2 days, followed by 5 days of refeeding with a normal diet, and collected fecal samples for 16S rRNA sequencing (Fig. 6a). Distinct alterations in microbial composition were observed under each condition, with consistent enrichment of

◀**Fig. 4**. Fecal microbiota transplantation induces shifts in gene expression and gut microbiota composition in MTNR mice. (**a**) Schematic diagram of the experiment. FMT was performed using the MTNR mice from Fig. 1 and Fig. 2, with n = 1 mouse per condition. Fecal material from mice recovered from restricted diets was suspended in PBS, and the supernatant was orally transplanted into MTNR mice on days 15 and 16. FMT was performed on one mouse per condition for both BALB/c and C57BL/6 J strains. The transplanted feces were collected from the cages of the corresponding mice shown in Fig. 1 and Fig. 2. **b**-**e**. The gene expression characteristics of the fecal microbiota transplantation (FMT) with feces derived from rMR, rTNR, or rMTNR groups compared to non-transplanted controls. (**b**) Volcano plots showing gene expression changes in recipient mice after FMT with feces derived from rMR, rTNR, or rMTNR groups, compared to non-transplanted controls. The x-axis represents the $\log_2$ fold change, and the y-axis indicates the adjusted p-values (padj). Differential expression analysis was performed using DESeq2, and the results were visualized using the EnhancedVolcano package in R. (**c**) Gene Ontology (GO) biological processes (BP) among the differentially expressed genes using the enrichGO function from the clusterProfiler package. Mouse gene Entrez IDs were used as input, and enrichment was assessed against the org.Mm.eg.db database. Significantly enriched GO terms were selected using Benjamini–Hochberg adjusted *p*-values and *q*-values less than 0.05. (**d**) Gene Set Enrichment Analysis (GSEA) of Gene Ontology Biological Processes (GO-BP) was performed using the gseGO function from the clusterProfiler package. Ranked gene lists based on differential expression were analyzed against the mouse GO-BP database (org.Mm.eg.db), identifying significantly enriched biological pathways ($p < 0.05$) with gene set sizes between 20 and 500. (**e**) Gene Set Enrichment Analysis (GSEA) was performed using the Reactome pathway gene sets from the Mouse MSigDB collection (m2.cp.reactome.v2024.1.Mm.entrez.gmt). Enrichment was conducted with the GSEA function using ranked gene lists derived from differential expression analysis. The detected enriched pathways based on normalized enrichment score (NES) were visualized. Color gradients represent *q*-values, indicating the statistical significance of pathway enrichment. (**f**) Gut microbiota composition of FMT groups analyzed at taxonomic level 6 using QIIME2.

Parabacteroides, members of the *Desulfovibrionaceae* and *Prevotellaceae* families across all nutrient-restricted groups (Fig. 6b–d). In addition, specific taxa were uniquely associated with particular diets: *Furicibacter* in MR, *Allobaculum* and *Methylobacterium* in TNR, *Christensenellaceae* in MTNR, *Coprococcus* and *Roseburia* in rMR, and *Sutterella* in rTNR (Fig. 6c, d). To determine whether FMT can modulate the microbiota regardless of restriction duration, we collected feces from mice subjected to 8 days of dietary restriction followed by 5 days of refeeding. Feces from the rMR, rTNR, and rMTNR groups were transplanted into mice currently undergoing MR, TNR, and MTNR diets, respectively, and the microbial composition was subsequently analyzed (Fig. 6e). FMT induced substantial changes in microbial profiles across all conditions, notably characterized by a marked increase in *Allobaculum* and *Desulfovibrionaceae* (Fig. 6f–h). Additionally, the rMTNR FMT group exhibited an enrichment of *Staphylococcus* (Fig. 6g, h). Collectively, these results suggest that dietary restriction might induce significant alterations in the gut microbiota irrespective of the duration of deprivation, and that FMT might effectively modulate microbial composition even in short-term restriction contexts.

Discussion

In this study, we investigated the impact of dietary deprivation of methionine, tryptophan and niacin on gene expression in the intestinal epithelium and the composition of the gut microbiota in mice. Our findings reveal that short-term deprivation of these micronutrients leads to significant alterations in the expression of genes involved in oxidative phosphorylation and fatty acid metabolism. Concomitantly, the gut microbial profile shifted toward an increased relative abundance of *Lactobacillus* species and a reduction in potentially pro-inflammatory taxa. These results suggest that host-microbiota interactions might be sensitive to fluctuations in specific micronutrients and that deprivation of methionine, tryptophan and niacin might reprogram intestinal homeostasis through both transcriptional and microbial mechanisms.

Activation of the MAPK and PI3K/AKT/mTOR signaling pathways has been reported to play a pivotal role in cancer progression and malignancy[44]. In the present study, we observed that deprivation of tryptophan and niacin led to a marked reduction in the gene expression of both MAPK and PI3K/AKT/mTOR pathways. These findings suggest that limiting the availability of these specific nutrients might contribute to the suppression of those pathway-related diseases. While CR has long been known to inhibit tumor progression[45], it is remarkable that the deprivation of just two micronutrients—tryptophan and niacin—might elicit comparable antitumor effects. In addition, previous studies have shown that methionine restriction suppresses the growth of gliomas[46]. Together with our results, this indicates that tryptophan and niacin deprivation might also play a critical role in the metabolic regulation of tumor suppression.

Our findings that deprivation of methionine, tryptophan, and niacin induces the activation and expansion of group 2 innate lymphoid cells (ILC2s) provide novel insights into the metabolic regulation of innate immunity. While ILC2s are traditionally associated with epithelial repair and allergic inflammation[47], recent evidence has emphasized their emerging role in antitumor immunity[48]. The observed link between nutrient-specific stress and ILC2 activation suggests that precise metabolic signals—notably the availability of essential amino acids and NAD^+ precursors—might act as key modulators of immune surveillance.

Previous studies have demonstrated that CR exerts antitumor effects through remodeling of the gut microbiome. In a colorectal cancer model, a CR regimen led to an increased abundance of *Bifidobacterium bifidum*, which enhanced interferon-γ^+ $CD8^+$ T cell activation and suppressed tumor growth[49]. Similarly, a significant reduction in tumor volume and weight was observed under CR conditions, accompanied by elevated levels of *Lactobacillus* and favorable shifts in gut microbial composition[50]. Metabolomic and microbiome

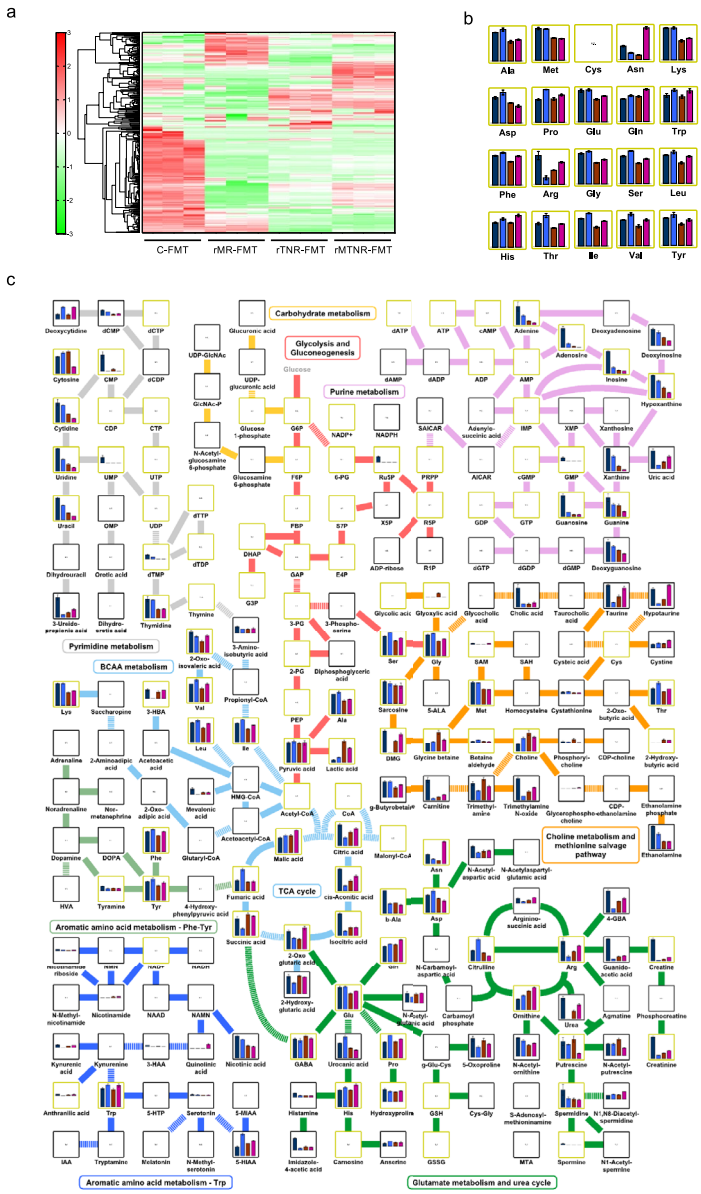

Fig. 5. Metabolomic profiling of recipient mice following fecal microbiota transplantation (FMT) using CE-TOFMS. **a**–**c**. Metabolomic analysis was performed on intestinal samples from BALB/c mice that received fecal transplants derived from normal diet controls (R), or recovery groups (rMR, rTNR, and rMTNR). Fecal microbiota samples were obtained from n = 1 mouse per condition and analyzed with n = 3 samples per condition. (**a**) Heatmap showing the relative abundance of detected metabolites in the intestines of FMT-recipient mice. (**b**) Quantification of amino acid levels across different groups. (**c**) Overview of major metabolic pathways with measured metabolite levels overlaid for each sample group.

analyses further revealed that CR enriched beneficial bacterial genera such as *Lactobacillus*, *Parabacteroides*, and *Roseburia*, which were associated with the suppression of tumor progression[51]. In this study, Short-term deprivation of methionine, tryptophan, and niacin resulted in an increased relative abundance of *Lactobacillus* species within the intestinal microbiota of mice. This observation suggests that selective nutrient limitation might exert microbiota-modulating effects comparable to those induced by CR.

FMT resulted in a marked reduction of adenine and guanine levels in the intestinal lumen, suggesting a metabolic remodeling of the gut environment. This reduction might confer several biological benefits. Purine nucleotides such as adenine and guanine are ultimately catabolized into uric acid and hypoxanthine, which have been associated with oxidative stress and pro-inflammatory responses in the gut[52]. Lower levels of these nucleobases might therefore mitigate inflammatory stimuli and support mucosal homeostasis. Additionally, rapidly proliferating tumor cells require a high supply of purine nucleotides for DNA replication and RNA synthesis[53]. Limiting the availability of extracellular purine bases might contribute to the suppression of tumor growth, particularly within the intestinal tract, by restricting a key metabolic substrate. Furthermore, certain

pathogenic or pro-tumorigenic bacteria utilize exogenous purines to enhance their fitness or virulence[54]; thus, the observed reduction might exert a selective pressure that favors beneficial microbial populations. Overall, these findings suggest that FMT-induced modulation of purine metabolism might represent an underappreciated mechanism by which gut microbiota interventions might exert immunometabolic effects.

It has been reported that BALB/c and C57BL/6 mice exhibit distinct immune regulatory mechanisms. BALB/c mice primarily depends on Foxp3$^+$ regulatory T cells for mucosal immune control, while C57BL/6 mice engages diverse regulatory pathways and express higher levels of checkpoint receptors[55]. Transcriptomic analyses further reveal strain-specific differences in immune cell recruitment and neuroinflammatory responses during infection[56]. Methionine deficiency has been reported to increase genetic instability in immune cells[57]. In contrast, tryptophan and niacin are essential for maintaining central nervous system function, serving as precursors for neurotransmitters and NAD$^+$, respectively[58,59]. In the present study, pathway analysis detected the reduction in the expression of genes associated with neurological disorders only in BALB/c mice under methionine-deficient conditions. On the other hand, pathway analysis revealed that deficiencies in tryptophan or niacin induced a similar downregulation of these genes in both BALB/c and C57BL/6 mice. These findings suggest that the effects of methionine deficiency on neurological gene expression might depend on immune status, whereas the effects of tryptophan and niacin deficiencies mignt appear to be independent of immune status.

Recent studies have revealed that low-tryptophan diet induces gut dysbiosis, characterized by increased abundances of *Acetatifactor*, *Enterorhabdus*, *Ruminococcaceae*, *Adlercreutzia*, *Marvinbryantia*, and *Allobaculum*, while reducing taxa such as *Lachnospiraceae*, *Mucispirillum*, *Blautia*, and *Limosilactobacillus reuteri*[25,60]. In addition, low-niacin diets in mice have been shown to increase the abundances of *S24-7* and *Ruminococcaceae*, while decreasing those of *Bacteroidaceae* and *Streptococcaceae*[61]. In the present study, the abundances of *S24-7* decreased under tryptophan- and niacin-deficient conditions, while *Allobaculum* increased after approximately two weeks of deficient diet in BALB/c mice but decreased in C57BL/6 mice. These findings suggest that combined nutrient deficiencies might either reflect or differ from the gut microbiota alterations observed under individual nutrient deficiencies, depending on the mouse strain.

Together, these findings highlight the importance of nutrient-specific interventions as modulators of both host intestinal gene expression and gut microbiota, suggesting that targeted dietary strategies might offer promising avenues for developing novel therapies in intestinal diseases. However, this study has some limitations. To minimize biological variability, we used only female mice. Previous studies have demonstrated that high-fat diet (HFD) feeding induces sex-specific metabolic outcomes in mouse models, with male mice consistently exhibiting greater susceptibility to weight gain, adiposity, and insulin resistance compared to females[62–64]. These findings emphasize the importance of considering sex-specific metabolic differences in experimental design. Future studies will be required to determine whether similar responses occur in male mice. While our study observed notable shifts in gut microbiome composition in response to dietary intervention, it remains unclear whether these microbial changes directly contributed to the alterations in host intestinal gene expression. It is possible that the dietary intervention itself acted as the primary driver of these effects. Previous studies have reported that a low amino acid diet induced comparable phenotypic changes even in mice with a depleted gut microbiota[65]. Therefore, in the present study, it is possible that the nutrient-deficient diets themselves directly influenced host intestinal gene expression, and this possibility warrants further investigation. Additionally, although we explored several conditions involving periods of nutrient deprivation followed by recovery, more optimal regimens might exist. Identifying and evaluating these alternative conditions remains an important direction for future investigation.

Methods

Diets

Methionine-, tryptophan-, and niacin-deficient diets were custom-formulated based on the AIN-93G standard by Dyets, Inc. Specifically, the methionine-deficient diet was provided as DYET#511,416, the tryptophan- and niacin-deficient diet as DYET#511,369, and the combined methionine/tryptophan/niacin-deficient diet as DYET#511,417 (see Supplementary Data S3 for composition details). These diets were gamma-irradiated and provided for use in the present study.

Ethics and animal experimental procedures

All animal procedures were approved by the Osaka University Animal Experiment Committee (Approval No. 30–011-053) and conducted in accordance with institutional guidelines. This study was also conducted and reported in accordance with the ARRIVE guidelines for reporting animal research. All cages and bedding were sterilized by autoclaving prior to use. Gamma-irradiated sterile chow was used for feeding. Eight-week-old wild-type female BALB/c Slc and C57BL/6 J mice (Japan SLC, Inc.) were housed in groups of five per cage under controlled conditions (23 °C, 12-h light/dark cycle). Mice were randomly assigned to control or dietary intervention groups and fed amino acid-defined diets deficient in methionine (MR), tryptophan and niacin (TNR), or a combination of all three (MTNR) for each experimental period. At the start of the nutrient-deficient diet intervention, mice were transferred to new sterilized cages and fed the nutrient-deficient diet. No cage changes were performed during the dietary intervention until fecal samples were collected. Then, mice were returned to a control diet and transferred to new sterilized cages, which were not changed again until the next fecal sample collection. In all experiments, food was available ad libitum in the cage, allowing mice to eat at any time. In the feeding control groups as well, standard chow was available ad libitum, allowing the mice to eat at any time. Fecal samples were collected on the final day of the depletion period for each dietary condition. One mouse was randomly selected from each cage, euthanized, and the intestines were subsequently harvested. In the recovery group, where mice were returned to a normal diet, fecal samples were collected at the end of the recovery period. One

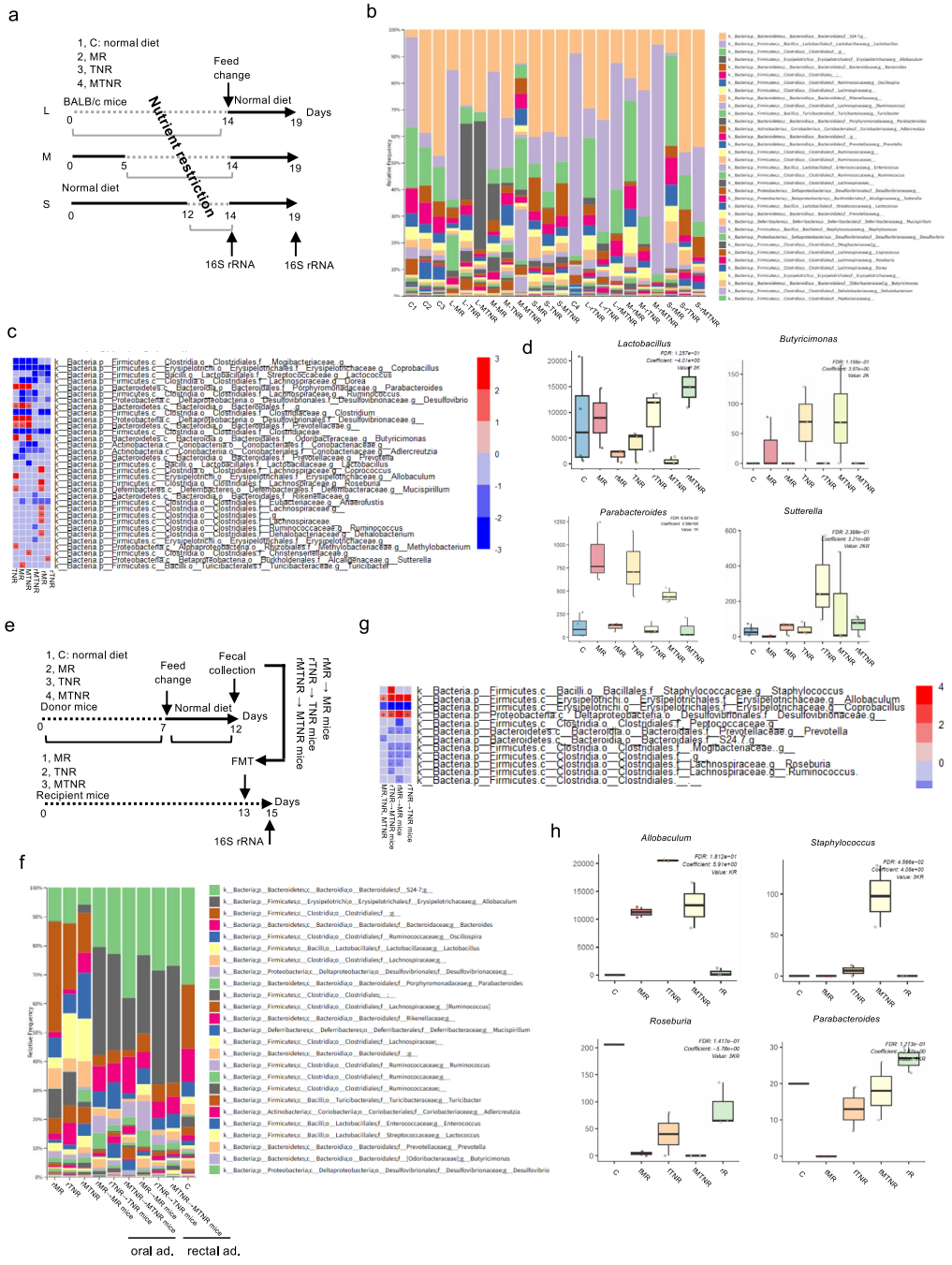

mouse was randomly selected from each cage, euthanized, and the intestines were collected thereafter. Sample collection was performed between 2 and 6 h after the beginning of the light phase. All euthanasia procedures were conducted in compliance with the American Veterinary Medical Association (AVMA) Guidelines for the Euthanasia of Animals (2020 edition) and the ARRIVE guidelines. Adult mice (6–12 weeks of age, body weight approximately 20 g) were euthanized using carbon dioxide (CO_2) inhalation. A gradual fill method was employed, with CO_2 introduced into the chamber at a flow rate of 0.5 L/min, reaching a final concentration of 40%, and maintained for 10 min. No anesthesia was administered prior to CO_2 exposure. Death was confirmed by the cessation of respiratory movement, absence of heartbeat, and lack of reflexes, including corneal and pedal withdrawal reflexes. All methods were carried out in accordance with the relevant guidelines and regulations.

Bulk RNA sequencing of intestinal tissues

Approximately 2 cm of the mid colon was collected for RNA extraction. A portion of the mouse colon was placed in 1 mL of ISOGEN (NIPPON GENE) and homogenized using a mixer. Following the addition of 0.2 mL chloroform, the mixture was centrifuged to separate the phases. RNA was extracted from the aqueous phase by isopropanol precipitation. The purified RNA was sent to the Microbiology Research Institute for RNA sequencing (RNA-seq). Although the RNA integrity number (RIN) was relatively low, RNA sequencing was performed due to the high value of the samples. Ribosomal RNA was depleted using the Ribo-Zero Plus rRNA Depletion Kit (Illumina), and libraries were prepared using the SMARTer Pico Input Mammalian Kit (TaKaRa).

◀**Fig. 6**. Gut microbiota changes depend on restriction duration and are transferable via fecal microbiota transplantation. (**a**) Schematic diagram of the experiment. BALB/c Mice were subjected to nutrient restriction for 14 days (L), 9 days (M), or 2 days (S). Fecal samples were collected at the end of the restriction period and five days after switching to a normal diet. 16S rRNA sequencing was performed on these samples. One mouse per condition ($n = 1$) was used. **b**–**d**. Microbiota profiles were analyzed in BALB/c mice subjected to methionine (MR), tryptophan and niacin (TNR), or the three substances (MTNR) restriction, as well as in mice recovered from these diets (rMR, rTNR, rMTNR). (**b**) Composition of the gut microbiota at taxonomic level 6 (genus level), visualized using QIIME2. C1, C2, and C3 are three fecal samples collected from a single control mouse on day 14. C4 is a fecal sample collected from a control mouse on day 19. (**c**) Correlation analysis between gut microbial taxa and dietary conditions using MaAsLin2. (**d**) Comparison of the relative abundance of diet-responsive microbial taxa across samples. (**e**) Schematic diagram of the experiment. After 7 days of nutrient restriction followed by 5 days on a normal diet, fecal samples from each recovery group (rMR, rTNR, rMTNR) were collected, suspended in PBS, and the supernatants were used for fecal microbiota transplantation (FMT). FMT was performed either orally or via the anus into recipient mice that had undergone 13 days of the corresponding nutrient-restricted diet (MR, TNR, or MTNR). Fecal samples were collected two days after FMT for 16S rRNA sequencing. One BALB/c mouse per condition ($n = 1$) was used. **f**–**h**. Gut microbiota analysis of BALB/c recipient mice under different durations of dietary restriction (distinct from Fig. 4). (**f**) Composition of the gut microbiota in each condition, visualized using QIIME2 at taxonomic level 6. Oral ad. and rectal ad. means oral administration and rectal administration, respectively. (**g**) Correlation analysis between dietary restriction and gut microbiota using MaAsLin2. (**h**) Comparative abundance of FMT-responsive microbial taxa across different samples. C: Normal diet group; rR: Recovery groups switched from restricted diets to normal diet (rMR, rTNR, and rMTNR); fMR: Fecal microbiota transplantation (FMT) from rMR mice to MR mice; fTNR: FMT from rTNR mice to TNR mice; fMTNR: FMT from rMTNR mice to MTNR mice.

Sequencing was performed using the MGI DNBSEQ-G400 platform in 100-base paired-end mode. Read mapping and gene expression quantification were performed using the Rhelixa RNA-seq pipeline (Rhelixa Inc.) on the supercomputer system at the National Institute of Genetics (NIG), Japan. Sequence quality of the FASTQ files was assessed using FastQC, and reads were trimmed based on quality scores using Trimmomatic. Trimmed reads were aligned to the mouse reference genome using Hisat2. The resulting SAM files were converted to BAM format with Samtools, and gene-level read counts were generated using featureCounts. Differential gene expression analysis was performed using DESeq2, and pathway enrichment analysis was conducted using clusterProfiler. Pathway annotations were based on the Kyoto Encyclopedia of Genes and Genomes (KEGG) database[66].

16S rRNA sequencing of gut microbiota

Fecal samples collected from each cage were submitted to the Microbiology Research Institute at the University of Osaka for 16S rRNA gene sequencing. Genomic DNA was extracted using the automated DNA extraction system, GENE PREP STAR PI-1200 system (Kurabo). Certain bacterial species have been reported to be more readily detected using the V1–V2 region than the V3–V4 region[67]. Therefore, the V1–V2 hypervariable regions of the 16S rRNA gene were amplified using the 27Fmod primer (5'-AGRGTTTGATCMTGGCTCAG-3') and the 338R primer (5'-TGCTGCCTCCCGTAGGAGT-3'). Sequencing was performed on the Illumina MiSeq platform using the MiSeq Reagent Kit v2 (500 cycles) in 251 bp paired-end mode. The resulting FASTQ files were processed using QIIME2 version 2020.2. Sequence denoising was conducted with the DADA2 plugin, and taxonomic assignments were made using the Greengenes 13_8 database. No rarefaction was performed; instead, counts were transformed to relative abundances for downstream compositional analysis. Differential abundance analysis of microbial taxa across dietary restriction conditions was performed using MaAsLin2 (Multivariable Association with Linear Models 2). This tool was applied to identify bacterial species whose relative abundances were significantly altered under each nutrient-deficient condition. Default settings were used, and taxa with a false discovery rate (FDR) < 0.05 were considered significantly associated with dietary interventions.

Single-cell RNA sequencing (scRNA-seq) of intestinal cells

Intestinal tissues from BALB/c mice shown in Fig. 1 were used to prepare single-cell suspensions for scRNA-seq. Tissues were minced in 3 mL of DMEM with 10% FBS, ulinastatin (2 μg/mL), and sivelestat (2 μg/mL) at 4 °C. Enzymatic digestion was performed with 25 mL of DMEM containing Collagenase D and DNase at 37 °C for 1 h. After digestion, 25 mL of DMEM with 10% FBS was added, and the suspension was filtered through 70 μm strainers and then passed through 10 μm strainers. The cell suspension was centrifuged, and the pellet resuspended in ACK buffer at 37 °C to lyse red blood cells. After lysis, cells were washed with PBS and resuspended in DMEM with 10% FBS. For scRNA-seq, cells were resuspended in PBS at 1000 cells/μL in 100 μL. scRNA-seq was conducted by the Microbiology Research Institute at the University of Osaka. Single-cell suspensions were processed using the Chromium Next GEM Single Cell 3' v3.1 kit (10 × Genomics) following the manufacturer's protocol. Libraries were sequenced on the Illumina NovaSeq 6000 platform in paired-end mode (read1: 50 bp; read2: 91 bp). Raw sequencing data were processed using Cell Ranger v6.0.0 (10 × Genomics) to generate gene expression matrices. Downstream analysis was performed in R using the Seurat package. Cells with fewer than 20% of unique molecular identifiers (UMIs) mapped to mitochondrial genes were retained for further analysis. Gene expression matrices from the control, MTNR, and rMTNR groups were imported and integrated using the SCTransform (SCT) normalization method. Integration features were selected using

SelectIntegrationFeatures with nfeatures = 3000, and dimensionality reduction was performed using uniform manifold approximation and projection (UMAP). Cell type annotation was carried out by identifying cluster-specific marker genes using the FindAllMarkers function in Seurat. Cell identities were assigned by comparing identified markers with published cell type-specific gene signatures. To explore cell–cell communication, ligand–receptor interaction analysis was performed using the CellChat package. Post-integration Seurat objects were converted into CellChat objects using the createCellChat function, and analyses were carried out following the CellChat developer's recommended pipeline. The processed scRNA-seq data are publicly available via Zenodo (https://zenodo.org/records/14226700).

Fecal microbiota transplantation (FMT)

Fecal microbiota transplantation (FMT) was performed using donor feces collected from recovery groups (rMR, rTNR, and rMTNR) as well as from control mice fed a normal diet. Fecal pellets were homogenized in sterile phosphate-buffered saline (PBS) and administered to recipient mice maintained on methionine-, tryptophan-, or combined methionine–tryptophan–niacin-deficient diets via a single oral gavage (200 µL per mouse). Recipient mice continued on their respective deficient diets throughout the duration of the FMT experiment. Fecal samples were collected from recipients at the end of the experiment for subsequent gut microbiota analysis.

Metabolomic profiling of fecal samples

Fecal samples from recipient BALB/c mice following fecal microbiota transplantation (FMT) in Fig. 4 were submitted to Human Metabolome Technologies, Inc. (HMT, Tsuruoka, Japan) for metabolomic analysis. Metabolite extraction and quantification were performed using capillary electrophoresis time-of-flight mass spectrometry (CE-TOFMS). Sample preparation, measurement, and data analysis were conducted according to HMT's standard protocols. Pathway illustrations were created by Human Metabolome Technologies, Inc.

Data availability

scRNA-seq data and RNA-seq data have been deposited in Zenodo and can be accessed at (https://zenodo.org/records/14226700) and (https://zenodo.org/records/15278786), respectively. The 16S rRNA sequencing data were analyzed using QIIME2, and the level 6 taxonomic profiles are presented in Supplementary Data S4, S5, S6, S8, and S9 of this manuscript. Quantitative data of metabolites are provided in Supplementary Data S7. The raw FASTQ files and processed files obtained from scRNA-seq, RNA-seq and 16S rRNA sequencing have been deposited in the Gene Expression Omnibus (GEO) as GSE301017, GSE300498 and GSE300499, respectively. The other datasets generated and analyzed during the current study are available from the corresponding author upon reasonable request.

Received: 7 May 2025; Accepted: 28 August 2025
Published online: 16 October 2025

References

1. Fontana, L. & Partridge, L. Promoting health and longevity through diet: from model organisms to humans. *Cell* **161**, 106–118 (2015).
2. Weindruch, R. & Walford, R. L. Dietary restriction in mice beginning at 1 year of age: effect on life-span and spontaneous cancer incidence. *Science* **215**, 1415–1418 (1982).
3. Wanagat, J., Allison, D. B. & Weindruch, R. Caloric intake and aging: mechanisms in rodents and a study in nonhuman primates. *Toxicol. Sci.* **52**, 35–40 (1999).
4. Masoro, E. J. Caloric restriction and aging: an update. *Exp. Gerontol.* **35**, 299–305 (2000).
5. Shimokawa, I. & Trindade, L. S. Dietary restriction and aging in rodents: a current view on its molecular mechanisms. *Aging. Dis.* **1**, 89–107 (2010).
6. Romashkan, S. V. et al. Safety of two-year caloric restriction in non-obese healthy individuals. *Oncotarget* **7**, 19124–19133 (2016).
7. Il'yasova, D. et al. Effects of 2 years of caloric restriction on oxidative status assessed by urinary F2-isoprostanes: The CALERIE 2 randomized clinical trial. *Aging Cell* **17**, e12719 (2018).
8. Waziry, R. et al. Effect of long-term caloric restriction on DNA methylation measures of biological aging in healthy adults from the CALERIE trial. *Nat. Aging* **3**, 248–257 (2023).
9. Redman, L. M. et al. Metabolic Slowing and Reduced Oxidative Damage with Sustained Caloric Restriction Support the Rate of Living and Oxidative Damage Theories of Aging. *Cell Metab.* **27**, 805-815.e804 (2018).
10. Heilbronn, L. K. et al. Effect of 6-month calorie restriction on biomarkers of longevity, metabolic adaptation, and oxidative stress in overweight individuals: a randomized controlled trial. *JAMA* **295**, 1539–1548 (2006).
11. Civitarese, A. E. et al. Calorie restriction increases muscle mitochondrial biogenesis in healthy humans. *PLoS Med.* **4**, e76 (2007).
12. Sun, J. C. et al. Time-restricted eating with calorie restriction on weight loss and cardiometabolic risk: a systematic review and meta-analysis. *Eur. J. Clin. Nutr.* **77**, 1014–1025 (2023).
13. Johnson, J. E. & Johnson, F. B. Methionine restriction activates the retrograde response and confers both stress tolerance and lifespan extension to yeast, mouse and human cells. *PLoS ONE* **9**, e97729 (2014).
14. Lee, B. C., Kaya, A. & Gladyshev, V. N. Methionine restriction and life-span control. *Ann. N. Y. Acad. Sci.* **1363**, 116–124 (2016).
15. Wang, S. Y. et al. Methionine restriction delays senescence and suppresses the senescence-associated secretory phenotype in the kidney through endogenous hydrogen sulfide. *Cell Cycle* **18**, 1573–1587 (2019).
16. Sanchez-Roman, I. & Barja, G. Regulation of longevity and oxidative stress by nutritional interventions: role of methionine restriction. *Exp. Gerontol.* **48**, 1030–1042 (2013).
17. Richardson, N. E. et al. Lifelong restriction of dietary branched-chain amino acids has sex-specific benefits for frailty and lifespan in mice. *Nat. Aging* **1**, 73–86 (2021).
18. Nakano, M. et al. Branched-chain amino acids enhance premature senescence through mammalian target of rapamycin complex I-mediated upregulation of p21 protein. *PLoS ONE* **8**, e80411 (2013).
19. Yang, Y. et al. Dietary methionine restriction improves the gut microbiota and reduces intestinal permeability and inflammation in high-fat-fed mice. *Food Funct.* **10**, 5952–5968 (2019).

20. Wu, G. et al. Dietary Methionine Restriction Ameliorated Fat Accumulation, Systemic Inflammation, and Increased Energy Metabolism by Altering Gut Microbiota in Middle-Aged Mice Administered Different Fat Diets. *J. Agric. Food Chem.* **68**, 7745–7756 (2020).
21. Wu, X. et al. Gut microbiota contributes to the methionine metabolism in host. *Front. Microbiol.* **13**, 1065668 (2022).
22. Gojda, J. & Cahova, M. Gut Microbiota as the Link between Elevated BCAA Serum Levels and Insulin Resistance. *Biomolecules* **11**, 1414 (2021).
23. Correia, A. S. & Vale, N. Tryptophan Metabolism in Depression: A Narrative Review with a Focus on Serotonin and Kynurenine Pathways. *Int. J. Mol. Sci.* **23**, 8493 (2022).
24. Krieger, I. & Statter, M. Tryptophan deficiency and picolinic acid: effect on zinc metabolism and clinical manifestations of pellagra. *Am. J. Clin. Nutr.* **46**, 511–517 (1987).
25. Yusufu, I. et al. A Tryptophan-Deficient Diet Induces Gut Microbiota Dysbiosis and Increases Systemic Inflammation in Aged Mice. *Int. J. Mol. Sci.* **22**, 5005 (2021).
26. Blankfield, A. A Brief Historic Overview of Clinical Disorders Associated with Tryptophan: The Relevance to Chronic Fatigue Syndrome (CFS) and Fibromyalgia (FM). *Int. J. Tryptophan. Res.* **5**, 27–32 (2012).
27. Gasperi, V., Sibilano, M., Savini, I. & Catani, M. V. Niacin in the Central Nervous System: An Update of Biological Aspects and Clinical Applications. *Int. J. Mol. Sci.* **20**, 974 (2019).
28. Kirkland, J. B. Niacin status and treatment-related leukemogenesis. *Mol. Cancer Ther.* **8**, 725–732 (2009).
29. Ahmed, A., Acharya, S., Shukla, S. & Ravikumar, V. Beyond the Bottle: Niacin Deficiency and Chronic Alcoholism. *Cureus* **15**, e49482 (2023).
30. Seal, A. J. et al. Low and deficient niacin status and pellagra are endemic in postwar Angola. *Am. J. Clin. Nutr.* **85**, 218–224 (2007).
31. Shah, G. M. et al. Biochemical assessment of niacin deficiency among carcinoid cancer patients. *Am. J. Gastroenterol.* **100**, 2307–2314 (2005).
32. Niño-Narvión, J. et al. NAD+ Precursors and Intestinal Inflammation: Therapeutic Insights Involving Gut Microbiota. *Nutrients* **15**, 2992 (2023).
33. Richard, D. M. et al. L-Tryptophan: Basic Metabolic Functions, Behavioral Research and Therapeutic Indications. *Int. J. Tryptophan. Res.* **2**, 45–60 (2009).
34. Williams, P. A. et al. Vitamin B(3) modulates mitochondrial vulnerability and prevents glaucoma in aged mice. *Science* **355**, 756–760 (2017).
35. Hara, T. et al. Fat and proteolysis due to methionine, tryptophan, and niacin deficiency leads to alterations in gut microbiota and immune modulation in inflammatory bowel disease. *Cancer Sci.* **115**, 2473–2485 (2024).
36. Wang, W., Yang, C., Wang, T. & Deng, H. Complex roles of nicotinamide N-methyltransferase in cancer progression. *Cell Death Dis.* **13**, 267 (2022).
37. Jung, I. R., Ahima, R. S. & Kim, S. F. Time-Restricted Feeding Ameliorates Methionine-Choline Deficient Diet-Induced Steatohepatitis in Mice. *Int. J. Mol. Sci.* **25**, 1390 (2024).
38. Zhong, W. et al. High-protein diet prevents fat mass increase after dieting by counteracting Lactobacillus-enhanced lipid absorption. *Nat. Metab.* **4**, 1713–1731 (2022).
39. Li, Y. et al. Differences in the Establishment of Gut Microbiota and Metabolome Characteristics Between Balb/c and C57BL/6J Mice After Proton Irradiation. *Front. Microbiol.* **13**, 874702 (2022).
40. Rodriguez-Rodriguez, N., Gogoi, M. & McKenzie, A. N. J. Group 2 Innate Lymphoid Cells: Team Players in Regulating Asthma. *Annu. Rev. Immunol.* **39**, 167–198 (2021).
41. Ademe, M. Benefits of fecal microbiota transplantation: A comprehensive review. *J. Infect. Dev. Ctries* **14**, 1074–1080 (2020).
42. Moreau, G. B., Naz, F. & Petri, W. A. Jr. Fecal microbiota transplantation stimulates type 2 and tolerogenic immune responses in a mouse model. *Anaerobe* **86**, 102841 (2024).
43. Osaki, H. et al. Clinical response and changes in the fecal microbiota and metabolite levels after fecal microbiota transplantation in patients with inflammatory bowel disease and recurrent Clostridioides difficile infection. *Fujita Med. J.* **7**, 87–98 (2021).
44. Hara, T. et al. Recent advances in noncoding RNA modifications of gastrointestinal cancer. *Cancer Sci.* **116**, 8–20 (2025).
45. Psara, E. et al. Intermittent Fasting against Cancer Development and Progression: Highlighting Potential Anticancer Molecular Mechanisms. *Anticancer Agents Med. Chem.* **23**, 1889–1909 (2023).
46. Qian, F., Xu, H., Zhang, Y., Li, L. & Yu, R. Methionine deprivation inhibits glioma growth through downregulation of CTSL. *Am. J. Cancer Res.* **12**, 5004–5018 (2022).
47. Kim, B. S., Wojno, E. D. & Artis, D. Innate lymphoid cells and allergic inflammation. *Curr. Opin. Immunol.* **25**, 738–744 (2013).
48. Wan, J. et al. ILC2-derived IL-9 inhibits colorectal cancer progression by activating CD8(+) T cells. *Cancer Lett.* **502**, 34–43 (2021).
49. Mao, Y. Q. et al. The antitumour effects of caloric restriction are mediated by the gut microbiome. *Nat. Metab.* **5**, 96–110 (2023).
50. Dai, X. C. et al. Calorie restriction remodels gut microbiota and suppresses tumorigenesis of colorectal cancer in mice. *Exp. Ther. Med.* **25**, 59 (2023).
51. Zhang, Y. et al. Modulation of intestinal metabolites by calorie restriction and its association with gut microbiota in a xenograft model of colorectal cancer. *Discov. Oncol.* **15**, 46 (2024).
52. Kaiko, G. E. et al. The Colonic Crypt Protects Stem Cells from Microbiota-Derived Metabolites. *Cell* **165**, 1708–1720 (2016).
53. Liu, J. et al. Targeting purine metabolism in ovarian cancer. *J. Ovarian. Res.* **15**, 93 (2022).
54. Li, F. et al. Fusobacterium nucleatum-triggered purine metabolic reprogramming drives tumorigenesis in head and neck carcinoma. *Discov. Oncol.* **14**, 120 (2023).
55. Hartmann, W., Blankenhaus, B., Brunn, M. L., Meiners, J. & Breloer, M. Elucidating different pattern of immunoregulation in BALB/c and C57BL/6 mice and their F1 progeny. *Sci. Rep.* **11**, 1536 (2021).
56. Bergersen, K. V., Barnes, A., Worth, D., David, C. & Wilson, E. H. Targeted Transcriptomic Analysis of C57BL/6 and BALB/c Mice During Progressive Chronic Toxoplasma gondii Infection Reveals Changes in Host and Parasite Gene Expression Relating to Neuropathology and Resolution. *Front. Cell Infect Microbiol.* **11**, 645778 (2021).
57. Binz, R. L. et al. Dietary Methionine Deficiency Enhances Genetic Instability in Murine Immune Cells. *Int. J. Mol. Sci.* **22**, 2378 (2021).
58. Tsujita, N., Akamatsu, Y., Nishida, M. M., Hayashi, T. & Moritani, T. Effect of Tryptophan, Vitamin B(6), and Nicotinamide-Containing Supplement Loading between Meals on Mood and Autonomic Nervous System Activity in Young Adults with Subclinical Depression: A Randomized, Double-Blind, and Placebo-Controlled Study. *J. Nutr. Sci. Vitaminol. (Tokyo)* **65**, 507–514 (2019).
59. Fricker, R. A., Green, E. L., Jenkins, S. I. & Griffin, S. M. The Influence of Nicotinamide on Health and Disease in the Central Nervous System. *Int. J. Tryptophan. Res.* **11**, 1178646918776658 (2018).
60. Rankin, L. C. et al. Dietary tryptophan deficiency promotes gut RORγt(+) Treg cells at the expense of Gata3(+) Treg cells and alters commensal microbiota metabolism. *Cell Rep.* **42**, 112135 (2023).
61. Susai, N., Kuroita, T., Kuronuma, K. & Yoshioka, T. Analysis of the gut microbiome to validate a mouse model of pellagra. *Biosci. Microbiota Food Health* **41**, 73–82 (2022).
62. Lefebvre, C. et al. Sex-dependent effects of a high fat diet on metabolic disorders, intestinal barrier function and gut microbiota in mouse. *Sci. Rep.* **14**, 19835 (2024).
63. Oraha, J., Enriquez, R. F., Herzog, H. & Lee, N. J. Sex-specific changes in metabolism during the transition from chow to high-fat diet feeding are abolished in response to dieting in C57BL/6J mice. *Int. J. Obes. (Lond)* **46**, 1749–1758 (2022).

64. Ota, K. et al. High Fat Diet Triggers a Reduction in Body Fat Mass in Female Mice Deficient for Utx demethylase. *Sci. Rep.* **9**, 10036 (2019).
65. Pak, H. H. et al. The Metabolic Response to a Low Amino Acid Diet is Independent of Diet-Induced Shifts in the Composition of the Gut Microbiome. *Sci. Rep.* **9**, 67 (2019).
66. Kanehisa, M. & Goto, S. KEGG: kyoto encyclopedia of genes and genomes. *Nucleic Acids Res.* **28**, 27–30 (2000).
67. Khogali, R. et al. Exploring the microbiomes of camel ticks to infer vector competence: insights from tissue-level symbiont-pathogen relationships. *Sci. Rep.* **15**, 5574 (2025).

Acknowledgements

Acknowledgments The authors thank all laboratory members for their valuable support and discussions. We acknowledge the Research Institute for Microbial Diseases, the University of Osaka, for assistance with RNA-seq, scRNA-seq, and 16S rRNA sequencing. Metabolomic profiling was performed by Human Metabolome Technologies, Inc., and RNA-seq data analysis was conducted using the Rhelixa RNAseq pipeline provided by Rhelixa, Inc. Computational analyses were partially carried out on the NIG supercomputer at the ROIS National Institute of Genetics.

Author contributions

T.H., S.M., D,M., Y.A., S.U., K.O., T.A., T.S., and H.I. designed the research. T.H., S.M., D,M., Y.A., S.U., K.O., T.A., and H.I. performed the research. T.H., S.M., D,M., K.O., and H.I. analyzed the data. T.H., S.M., D,M., S.U., K.O., T.A., T.S., M.K. and H.I. wrote the manuscript. T.H., S.M., D,M., S.R., S.U., and H.I. revised the manuscript. M.K. and H.I. supervised the work. All authors have read and agreed to the published version of the manuscript.

Funding

This work was supported in part by a Grant-in-Aid for Scientific Research from the Ministry of Education, Culture, Sports, Science and Technology (grant nos. 19K22658, 20H00541, 21K19526, 22H03146, 22K19559, 23K19505, 23K18313, 23KK0153, 24K22144, and 16H06279 (PAGS)), and Japan Agency for Medical Research and Development (AMED) (grant nos. JP23ym0126809 and JP24ym0126809). Partial support was offered by Princess Takamatsu Cancer Research Fund. (2023), to H.I.

Declarations

Competing interests

Partial institutional endowments were received from Hirotsu Bio Science Inc. (Tokyo, Japan); Kinshu-kai Medical Corporation (Osaka, Japan); Kyowa-kai Medical Corporation (Osaka, Japan); IDEA Consultants Inc. (Tokyo, Japan); and Unitech Co. Ltd. (Chiba, Japan). K.O. is an employee of IDEA Consultants Inc. T.A. is an employee of Unitech Co. Ltd. The remaining authors have no competing interests for the present research.

Additional information

Supplementary Information The online version contains supplementary material available at https://doi.org/10.1038/s41598-025-18046-2.

Correspondence and requests for materials should be addressed to H.I.